7-15-2022

Post-stroke reorganization of transient brain activity characterizes deficits and recovery of cognitive functions

Elvira Pirondini
University of Geneva

Nawal Kinany
University of Geneva

Cécile Le Sueur
Ecole Polytechnique Fédérale de Lausanne

Joseph C Griffis
Washington University School of Medicine in St. Louis

Gordon L Shulman
Washington University School of Medicine in St. Louis

See next page for additional authors

NeuroImage 255 (2022) 119201

Contents lists available at ScienceDirect

NeuroImage

journal homepage: www.elsevier.com/locate/neuroimage

Post-stroke reorganization of transient brain activity characterizes deficits and recovery of cognitive functions

Elvira Pirondini[a,b,c,d,e,1], Nawal Kinany[a,b,f,1], Cécile Le Sueur[b], Joseph C. Griffis[g], Gordon L. Shulman[g], Maurizio Corbetta[g,h,i,j,k,l], Dimitri Van De Ville[a,b,*]

[a] Department of Radiology and Medical Informatics, University of Geneva; 1211 Geneva, Switzerland
[b] Medical Image Processing Laboratory, Center for Neuroprosthetics, Institute of Bioengineering, Ecole Polytechnique Fédérale de Lausanne (EPFL); 1202 Geneva, Switzerland
[c] Department of Physical Medicine and Rehabilitation, University of Pittsburgh; Pittsburgh, PA, USA
[d] Rehabilitation Neural Engineering Laboratories, University of Pittsburgh; Pittsburgh, PA, USA
[e] Department of BioEngineering, University of Pittsburgh; Pittsburgh, PA, USA
[f] Bertarelli Foundation Chair in Translational Neuroengineering, Center for Neuroprosthetics, Institute of Bioengineerin, Ecole Polytechnique Fédérale de Lausanne (EPFL); 1202 Geneva, Switzerland
[g] Department of Neurology, Washington University School of Medicine, St. Louis; MO, 63110, USA
[h] Department of Radiology, Washington University School of Medicine, St. Louis; MO, 63110, USA
[i] Department of Anatomy and Neurobiology, Washington University School of Medicine, St. Louis; MO, 63110, USA
[j] Department of Bioengineering, Washington University School of Medicine, St. Louis; MO, 63110, USA
[k] Department of Neuroscience and Padua Neuroscience Center, University of Padua; Padua, Italy
[l] Venetian Institute of Molecular Medicine (VIMM); Padua, Italy

ARTICLE INFO

Keywords:
fMRI
Dynamic functional connectivity
Test-retest reliability
Stroke

ABSTRACT

Functional magnetic resonance imaging (fMRI) has been widely employed to study stroke pathophysiology. In particular, analyses of fMRI signals at rest were directed at quantifying the impact of stroke on spatial features of brain networks. However, brain networks have intrinsic time features that were, so far, disregarded in these analyses. In consequence, standard fMRI analysis failed to capture temporal imbalance resulting from stroke lesions, hence restricting their ability to reveal the interdependent pathological changes in structural and temporal network features following stroke. Here, we longitudinally analyzed hemodynamic-informed transient activity in a large cohort of stroke patients (n = 103) to assess spatial and temporal changes of brain networks after stroke. Metrics extracted from the hemodynamic-informed transient activity were replicable within- and between-individuals in healthy participants, hence supporting their robustness and their clinical applicability. While large-scale spatial patterns of brain networks were preserved after stroke, their durations were altered, with stroke subjects exhibiting a varied pattern of longer and shorter network activations compared to healthy individuals. Specifically, patients showed a longer duration in the lateral precentral gyrus and anterior cingulum, and a shorter duration in the occipital lobe and in the cerebellum. These temporal alterations were associated with white matter damage in projection and association pathways. Furthermore, they were tied to deficits in specific behavioral domains as restoration of healthy brain dynamics paralleled recovery of cognitive functions (attention, language and spatial memory), but was not significantly correlated to motor recovery. These findings underscore the critical importance of network temporal properties in dissecting the pathophysiology of brain changes after stroke, thus shedding new light on the clinical potential of time-resolved methods for fMRI analysis.

Abbreviations: fMRI:, functional magnetic resonance imaging; rs-fMRI:, resting-state fMRI; FC:, functional connectivity; dFC:, dynamic FC; iCAP:, innovation-driven coactivation patterns; PCA:, principal component analysis; CSF:, cerebrospinal fluid; TA:, total activation; AUC:, area under the receiver operation characteristics curve; LDA:, linear discriminant analysis; PLSC:, partial least squares correlation; FDR:, false discovery rate; DMN:, default mode network; EMC:, extreme capsule; IFOF:, inferior fronto-occipital fasciculus.

* Corresponding author.
E-mail addresses: elvirap@pitt.edu (E. Pirondini), dimitri.vandeville@epfl.ch (D. Van De Ville).

[1] These authors contributed equally to this work.

https://doi.org/10.1016/j.neuroimage.2022.119201.
Received 7 October 2021; Received in revised form 24 March 2022; Accepted 7 April 2022
Available online 9 April 2022.

1. Introduction

The mammalian brain, even in the absence of explicit task, operates through the continuous integration and segregation of signals from different brain areas. Since the landmark work from Fox and colleagues in 2005 (Fox et al., 2005), functional magnetic resonance imaging (fMRI) performed at rest has become one of the most prominent methods to investigate intrinsic brain activity and its relationship with behavior or psychopathology (Van Den Heuvel and Pol, 2010; Lee et al., 2013; Bolton et al., 2020). These task-free resting-state paradigms could potentially be advantageous to measure pathological brain changes, as they can be readily deployed, even with patients unable to match control performance due to motor and cognitive impairment (Krakauer, 2004; Krakauer, 2007).

Analysis of resting-state fMRI (rs-fMRI) has so far mostly relied on measuring inter-regional (or voxel- or vertex-level) connectivity by means of Pearson correlation between time-series from a set of predefined regions of interest (a.k.a. *static* functional connectivity). In these studies, information exchange between neuronal populations of different regions is assumed to engender stronger statistical dependency stationary over time. Nevertheless, the human brain is a dynamic system that fluctuates at the time scale of milliseconds (Van Den Heuvel and Pol, 2010). Therefore, *static* connectivity approaches, despite their methodological simplicity and ease, may miss features reflecting the inherent dynamic nature of the brain. In the last decade, several time-resolved approaches have thus been proposed to investigate the so-called *dynamic* functional connectivity (dFC) (see (Preti et al., 2017) for a review). They have been demonstrated to provide benefits over *static* methods, notably to study cognition and psychiatric disorders (Preti et al., 2017; Cohen, 2018; Karahanoğlu and Van De Ville, 2017; Hutchison et al., 2013). Besides, deeming non-stationarity enables a more accurate description of the modular interactions occurring between brain functional networks and their anatomical substrate (Bullmore and Sporns, 2009).

Stroke is one of the major neurological disorders in Western societies and a leading cause of long-term disabilities. Ranging from motor to cognitive deficits, these disabilities arise from both focal structural changes (tied to the injury) and widespread functional alterations in inter-regional connectivity (Siegel et al., 2016; Salvalaggio et al., 2020), as theorized under the concept of *connectional diaschisis* (Carrera and Tononi, 2014). Structural and functional abnormalities combine in an interdependent manner to generate both deficits and recovery processes. Considering the complexity of these interactions, time-resolved FC approaches, which capture spatial *and* temporal properties of brain networks, could help unravel the intertwine between structural disruptions and lesion-induced dynamic changes in large-scale functional networks. Coupled to behavioral and clinical assessments, these methods could further elucidate the nature of pathological changes occurring after stroke, possibly supporting our understanding of recovery processes. However, while moving from stationary to dynamic functional connectivity estimates is an important methodological endeavor, it faces additional challenges such as test-retest reliability, which appears to be even more critical for time-tailored than for classical methods (Cohen, 2018; Zhang et al., 2018). Lack of test-retest reliability of fMRI measures challenges the interpretability of the current clinical findings, particularly with regard to changes over time.

Previously, a handful of studies have employed time-tailored methods to explore the neural correlates of stroke (Bonkhoff et al., 2020; A.K. Bonkhoff et al., 2021; A.K. Bonkhoff et al., 2021; Hu et al., 2018; Obando et al., 2019; Duncan and Small, 2018; Chen et al., 2018) showing evidence in favor of a dynamic reconfiguration of brain networks following stroke. However, they relied on small sample sizes and focused solely on specific neurological symptoms (i.e., mostly motor deficits), limiting the generalizability of their findings (Woo et al., 2017). Besides, they relied on *a priori* selection of brain regions, which limits the identification of alternative areas that may be recruited into a network (Carter et al., 2012), and on time-windowed estimates, which confine the investigation to slow changes in connectivity (Preti et al., 2017).

Here, we leveraged a recent dynamic FC framework, i.e., the innovation-driven coactivation patterns (iCAP) framework (Karahanoğlu and Van De Ville, 2015; A. Tarun et al., 2020; Zöller et al., 2019; D.M. Zöller et al., 2018; Zoeller et al., 2019; Piguet et al., 2021), to overcome these limitations and investigate whether spatial and temporal properties of large-scale brain networks following stroke correlate with anatomical damage and behavioral recovery. Importantly, the iCAP method relies on a data-driven approach that employs single frames without a priori selection of regions of interest. In addition, it includes a hemodynamic-informed deconvolution step, which confers to this framework the unique potential of identifying large-scale brain networks that can be spatially *and* temporally overlapping. These procedures were previously demonstrated to allow disentangling the spatiotemporal organization of brain (Karahanoğlu and Van De Ville, 2015) and spinal cord activity (Kinany et al., 2020; Kinany et al., 2022) with a finer level of detail, which is beneficial to capture spatial and temporal properties of brain networks. We applied the iCAP framework to an extensive dataset including healthy controls (n = 19) scanned in two sessions at three months apart and stroke patients (n = 103) scanned at different points in time after-lesion (i.e., 1–2 weeks, 3 months and 1 year) and with different neurological syndromes (i.e., ranging from motor to cognitive deficits). Part of the data were already presented in previous publications demonstrating the validity of the dataset (Siegel et al., 2016; Salvalaggio et al., 2020; Siegel et al., 2018; Griffis et al., 2020; Griffis et al., 2019; Corbetta et al., 2015; Ramsey et al., 2017). We first assessed test-retest reliability of spatial and temporal properties of the extracted brain networks in the healthy subjects, so as to confirm the robustness of the metrics of interest. Building upon these results, we then compared these control values with those derived from the brain networks of stroke patients. While the spatial patterns of the obtained large-scale functional brain networks were preserved after stroke, lesions disrupted their temporal durations, emphasizing the prospects of exploiting time-resolved fMRI methods. Importantly, these altered durations were *i)* proportional to the percentage of disrupted white matter fibers; *ii)* specific to the neuropsychological deficit; *iii)* correlated with functional improvements; and *iv)* restored over time proportionally to the recovery of deficits.

This is the first time that a time-resolved approach is deployed in a large cohort of stroke patients, which were evaluated longitudinally with a comprehensive set of multi-domain clinical assessments. Using the iCAP framework, we revealed important aspects of post-lesional reorganization of functional dynamics, in relation to anatomy and to behavioral changes. We posit that understanding the nature of this relationship is pivotal to grasp the multifaceted reorganization mechanisms that occur following stroke, and that are directly involved in recovery (Woo et al., 2017; Haller et al., 2014; Allali et al., 2018; Ward, 2015; Guggisberg et al., 2019).

2. Material and methods

2.1. Participants

All participants gave their written informed consent to participate in accordance with the Declaration of Helsinki, and the study was approved by the Institutional Review Board at Washington University in St. Louis. The complete data collection protocol is described in detail elsewhere (Corbetta et al., 2015). Part of the data were used in previous publications (Siegel et al., 2016; Salvalaggio et al., 2020; Siegel et al., 2018; Griffis et al., 2020; Griffis et al., 2019; Corbetta et al., 2015; Ramsey et al., 2017). Data from 127 first-time stroke patients with clinical evidence of impairment and data from 21 demographically matched healthy controls were considered for inclusion in the analyses

(**Table S1**). Healthy adults matched the stroke population by age, gender, handedness, and level of education (see (Siegel et al., 2016) for details in inclusion and exclusion criteria for the two population groups).

From the initial sample of 148 subjects, $n = 24$ patients and $n = 2$ healthy subjects were excluded from the analysis because of excessive motion (> 60% of volumes with a framewise displacement of more than 0.5 mm (Power et al., 2012)) or because of a low number of significant innovation frames (< 131 significant innovation frames over a total of 808 vol). Importantly, patients and controls had comparable head movements (mean frame displacement: 0.28 ± 0.009 mm for patients and 0.32 ± 0.03 mm for healthy subjects, respectively, non-significant Wilcoxon Ranksum Test; and percentage of volumes with framewise displacement of more than 0.5 mm ± STD: 16.11 ± 16.09% and 16.55 ± 15.04%, for patients and healthy subjects, respectively, non-significant Wilcoxon Ranksum Test). This confirms that the differences found in the iCAP characteristics are not resulting from differences in head movement between the two groups.

2.2. Experimental protocol

Patients underwent a maximum of three testing sessions (**Table S1**): within 1–2 weeks ($n = 103$), 3 months ($n = 72$), and 12 months ($n = 54$) after the lesion (see (Siegel et al., 2018) for motivations and percentages of patients lost over the three time points). Healthy control subjects participated in two testing sessions three months apart in order to assess test-retest reliability of the extracted measures. Each testing session consisted of seven resting state fMRI runs, each including 128 vol (30 min total) and a neuropsychological assessment. Imaging and behavioral testing sessions were usually performed on the same day.

2.3. Neuropsychological assessment

Participants underwent a comprehensive battery of 44 behavioral tests across four behavioral domains language, memory, motor, attention and visual function, chosen to represent a wide range of the most commonly identified deficits in stroke patients. Scores were only recorded for tasks that subjects were able to complete. Therefore, different domains include different numbers of subjects (**Table S1**). In order to isolate clusters of deficits based on these different measures, we applied principal component analysis (PCA) on the behavioral data for each domain separately (e.g., motor, language, attention, spatial memory, and verbal memory) following our previous method (Corbetta et al., 2015; Ramsey et al., 2017)) (see *Behavioral domain scores* for details).

2.4. Imaging acquisitions

All imaging was performed using a Siemens 3T Tim-Trio scanner and a standard 12-channel head coil. The MRI protocol included structural and functional scans. Structural scans included: (i) a sagittal T1-weighted MPRAGE (TR = 1950 msec, TE = 2.26 msec, flip angle = 90°, voxel size = 1.0 × 1.0 × 1.0 mm); (ii) a transverse T2-weighted turbo spin echo (TR = 2500 msec, TE = 435 msec, voxel size = 1.0 × 1.0 × 1.0 mm); and (iii) sagittal fluid attenuated inversion recovery (FLAIR) (TR = 750 msec, TE = 32 msec, voxel size = 1.5 × 1.5 × 1.5 mm). Resting state functional scans were acquired with a gradient echo EPI sequence (TR = 2000 msec, TE = 27 msec, 32 contiguous 4-mm slices, 4 × 4 mm in-plane resolution) during which participants were instructed to fixate a small cross white cross centered on a screen with a black background in a low luminance environment.

2.5. Behavioral domain scores

Dimensionality reduction was performed on the behavioral data as described in detail in (Corbetta et al., 2015; Ramsey et al., 2017). First, tasks were categorized as attention, spatial memory, verbal memory, language, and motor. A PCA was run on the behavioral data of the session at 1–2 weeks post-lesion and the first component was used as a domain score for each category separately. The component scores for subsequent time points and for the age-matched controls were generated by normalizing the original data based on the sub-acute values and projecting them in the PCA space. Then, each of the components and time-points was z-scored based on the first measurement of the healthy control group, allowing comparisons across timepoints and behavioral domains. Patients with a score >/< 2 standard deviations were identified as “patients with/without severe acute deficits”. For each behavioral domain, we followed the same procedure as (Ramsey et al., 2017) and conducted an ANOVA across the three timepoints comparing patients with and without severe acute deficits. PCA components for the different behavioral domains were similar to those previously reported (Corbetta et al., 2015; Ramsey et al., 2017). Specifically, in attention, the first component described 24.7% of variance and was strongly related to measures of attentional field bias such as the total number of miss items in Mesulam cancelation test ($r = 0.61$), and the accuracy ($r = 0.85$) and reaction time ($r = 0.72$) in the Posner task. For the motor domain, the first two components (explained variance 40.0% and 32.2% respectively) correlated with left and right motor function. In language the first component accounted for 77.3% of the variance and correlated with tasks of auditory comprehension, expression, and reading ($r > 0.81$). Finally, for spatial memory the first component (explained variance 61%) was correlated with measures of visuospatial memory such as immediate ($r = 0.87$) and delayed recall ($r = 0.90$) of visual information on the Brief Visuospatial Memory Test; whereas for verbal memory the first factor (explained variance 74.9%) correlates with measures from the Hopkins Verbal Learning Test such as delayed recall of words ($r = 0.96$). Importantly, results were similar if considering all the time points in the PCA. Indeed, the correlation between the recovery calculated from the PCA that considered only the first time point and the recovery calculated from the PCA that considered all time points was high (mean ± STD over behavioral domains: 0.96 ± 0.05). This further supports that the post-stroke behavioral impairment is genuinely the main source of population variance in the study.

2.6. fMRI data pre-processing

MRI scans were pre-processed using a pipeline adapted from our previous studies (A. Tarun et al., 2020; Zöller et al., 2019; Zoeller et al., 2019) that used SPM8 (http://www.fil.ion.ucl.ac.uk/spm/). After realignment of functional scans, we applied spatial smoothing with an isotropic Gaussian kernel of 5-mm full-width at half-maximum and coregistered structural scans to the functional mean. Individual tissue (white and gray matter, and cerebrospinal fluid (CSF)) maps were segmented from the T1 image. Then, the first ten functional scans were discarded, resulting in $T = 118$ vol per run (for a total of 826 vol per subject – i.e., 118×7 runs). The following sources of spurious variance were regressed out from these BOLD time series: (i) six parameters obtained by rigid body correction of head motion, (ii) average white matter and CSF signals. Finally, for each session fMRI runs were spatially realigned to the functional mean of the first run.

2.7. Extraction of large-scale brain networks

In order to extract large-scale brain networks and their temporal characteristics we deployed the iCAP framework (Karahanoğlu and Van De Ville, 2015) (**Fig. 1**), which is based on the detection of significant changepoints in deconvolved fMRI time series. For this, we first applied the Total Activation framework (TA (Karahanoğlu et al., 2013)), which applies hemodynamically informed deconvolution to the pre-processed fMRI time series (native space) of each subject and run separately, to reliably retrieve activity-inducing time courses. Then, for each subject and session, activity-inducing time courses of all runs were concatenated, removing three volumes at each intersect (i.e., 808 vol kept in total per

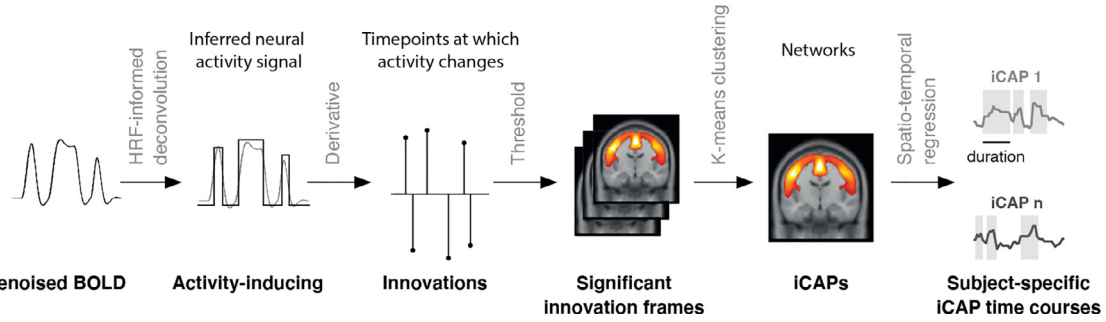

Fig. 1. Dynamic functional connectivity framework | Functional images from individual subjects are denoised to circumvent the effect of various sources of noise. The hemodynamic blur is subsequently removed using hemodynamic-informed deconvolution, which reveals the activity-inducing signals. The innovation frames are then obtained by temporal derivation. A two-step thresholding (temporal and spatial) is applied to select significant innovation frames (i.e., transients), which undergo temporal clustering over subjects to obtain stable iCAPs. The latter are fitted back to the individual activity inducing signals to recover temporal profiles of the iCAPs for further time-resolved analysis. For each participant, session, and iCAP, we then computed the average duration over the total acquisition length.

subject and session) and activation change-points were computed as the temporal derivative of these activity-inducing signals. Significant activation change-points or innovations frames (i.e., frames with significant transitioning activities - transients) were selected with a two-step thresholding procedure with *temporal* and *spatial thresholds* selected based on previous work (Karahanoğlu and Van De Ville, 2015; A. Tarun et al., 2020; Zöller et al., 2019; D.M. Zöller et al., 2018; Zoeller et al., 2019; Piguet et al., 2021; Kinany et al., 2020). This two-step thresholding allowed to select only frames that contained significantly transient activity and to avoid including spurious connectivity patterns. The purpose of the *temporal thresholding* was, for each voxel, to find the time points where the activity was significantly high (i.e., positive)/low (i.e., negative). For that, we defined a threshold based on phase-randomized surrogate data. Specifically, a surrogate distribution was obtained by applying TA on phase randomized data and a 1% confidence interval was used to select significant voxels. We did that for all voxels and we thus obtained, for each time point, a map of significant positive or negative transients, i.e., a map of regions that are jointly activating (i.e., positive frames) or jointly deactivating (i.e., negative frames). We then applied *spatial thresholding* on these maps, to only select those that have more than 5% of significant voxels (i.e., transients). Transients were then normalized to the MNI space considering the lesion mask as a prior for an additional tissue class in the segmentation procedure (Brett et al., 2001), concatenated across all subjects (i.e., patients and healthy subjects) and sessions, as also done in our previous work comparing patients and healthy subjects (Zöller et al., 2019; Piguet et al., 2021). Transients were then fed into a temporal k-means clustering to obtain large-scale resting-state networks, the iCAPs. The optimum number of clusters was determined by evidence accumulation (Fred and Jain, 2002; Fred and Jain, 2005) (see **Figures S2a**). Briefly, the k-means clustering was done for K values ranging from 10 to 24, in order to obtain a co-association matrix summarizing how often two frames were clustered together. A second phase of clustering was performed using this co-association matrix and, this time, hierarchical clustering with two different linkage functions (average and weighted). We then computed the percentage of agreement between these two linkage functions, as well as with the k-means solution. The number of iCAPs was chosen as the number that showed the highest percentage of agreement, thus resulting in the extraction of 16 iCAPs (**see Figure S2a**). Finally, subject-specific iCAP time courses were obtained for each subject and session by transient-informed spatiotemporal back-projection of the 16 spatial maps (i.e., the large-scale resting-state networks extracted when clustering together transients concatenated across all patients and healthy subjects) onto the individual activity-inducing signals (**Figure S2b** and (D.M. Zöller et al., 2018)). Matlab code for the application of the whole framework can be found at https://www.c4science.ch/source/iCAPs.

2.8. Extraction of temporal properties

In order to extract the iCAPs temporal properties, for each subject and session, the subject-specific iCAPs time courses were Z-scored and thresholded ($|Z| > 1$) to highlight active and de-active time points. The choice of this particular threshold was motivated by previous works that implemented TA and iCAP framework (Zöller et al., 2019; D.M. Zöller et al., 2018; Kinany et al., 2020). For each iCAP, subject, and session we then computed the average duration of each iCAP occurrence as the number of time points that a iCAP was active or de-active.

2.9. Lesion masking

Individual T1 MRI images were registered to the MNI brain using FSL (FMRIB Software Library) FNIRT tool (Andersson et al., 2007). We used the lesion masks already reported in our previous studies (Siegel et al., 2016; Salvalaggio et al., 2020; Siegel et al., 2018; Griffis et al., 2020; Griffis et al., 2019; Ramsey et al., 2017). In order to obtain them, lesions were manually segmented on individual structural MRI images obtained 1–2 weeks post-lesion using the Analyze biomedical imaging software system (Robb and Hanson, 1991). Special attention was given to distinguish lesion from CSF, hemorrhage from surrounding vasogenic edema, and to identify the degree of periventricular white matter damage present. In hemorrhagic strokes, edema was included in the lesion. The staff that was involved in segmenting or in reviewing the lesions (M.C. and Alexandre Carter) was blind to the individual behavioral data. We computed the topography of the lesion as the sum of all lesion masks over the 103 patients.

2.10. White matter tracts disconnections

In order to quantify the damages to the different cortical and subcortical white matter tracts, we used our previous approach (Griffis et al., 2020; Griffis et al., 2019). Specifically, for each patient, we intersected the lesion mask with a streamline tractography atlas and we quantified the proportion of streamlines disconnected for each tract. For the tractography atlas, we used a publicly available diffusion MRI streamline tractography atlas (Yeh et al., 2018), which consisted of 70 tracts: 65 neuroanatomically defined fiber bundles corresponding to commissural, association, projection, brainstem, and cerebellar pathways (cranial nerves were not included), and the corpus callosum split into 5 segments (Griffis et al., 2020; Griffis et al., 2019; Tzourio-Mazoyer, 2002)

2.11. Statistical analysis

2.11.1. Stability of iCAP spatial patterns

First, we obtained iCAP spatial patterns for each individual and session by averaging significant innovation frames belonging to the

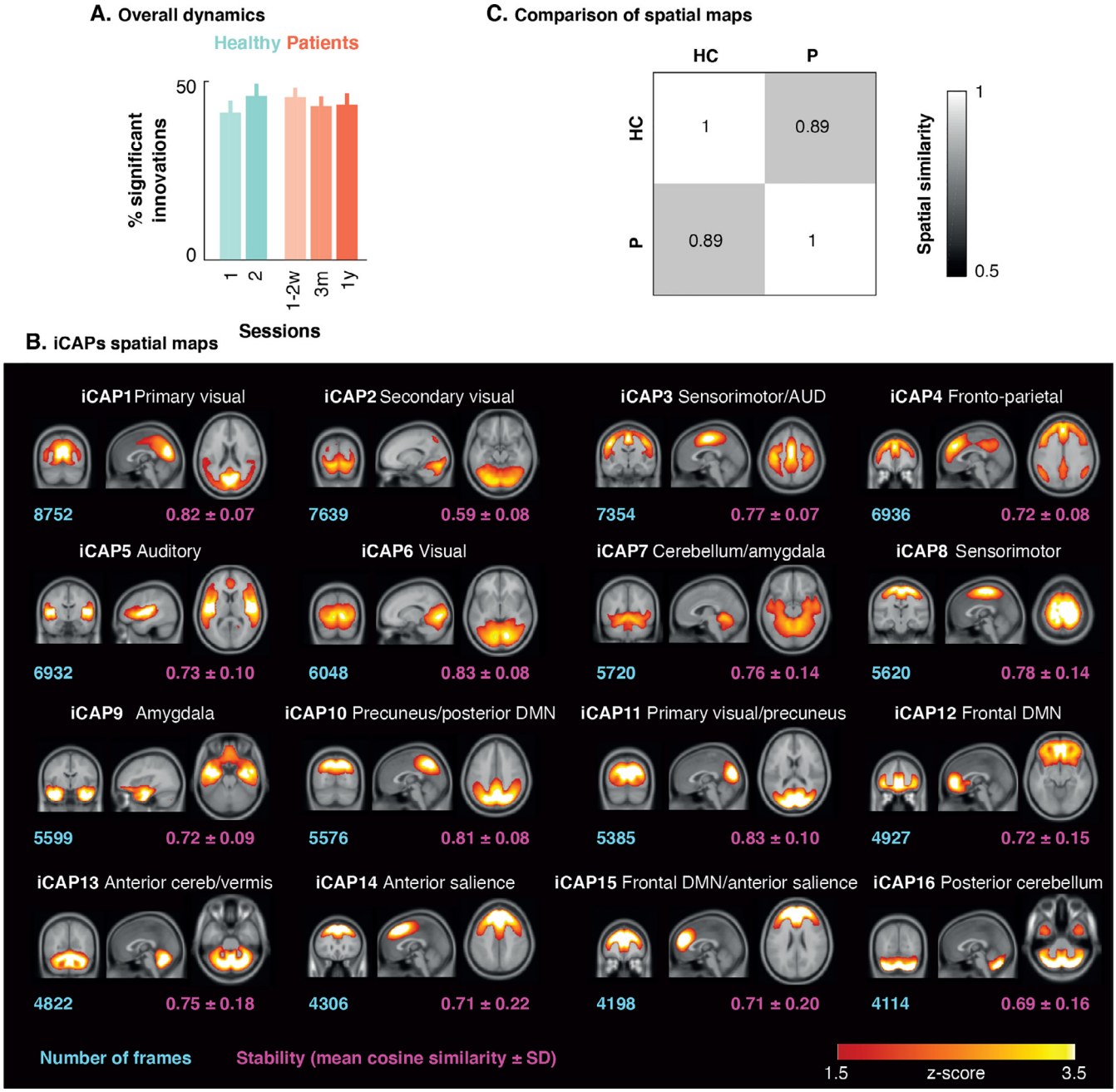

Fig. 2. iCAP networks and spatial features | A. Number of transients (or significant innovation frames) including both positive and negative frames expressed in percentage of the total number of frames for the two sessions of the healthy control subjects (in cyan) and for the three sessions of the stroke patients (in orange). **B.** Spatial patterns (displayed in Montreal Neurological Institute coordinates) for the 16 innovation-driven coactivation patterns (iCAPs) retrieved from all subjects, including both sessions of the healthy control subjects and the three sessions of the stroke patients. Blue values denote the total number of significant innovation frames of each cluster (i.e., iCAP) and purple values indicate the stability of each cluster calculated as the mean cosine similarity from the centroid over subjects both healthy controls and patients (mean ± SD over subjects) (see **Figure S3d** for a separated analysis between healthy subjects and patients). AUD, auditory; DMN, default mode network; cereb, cerebellum. **C.** Dice coefficients between iCAP spatial patterns for healthy controls (HC) and patients (P) averaged over the 16 iCAPs.

corresponding subject and session. For each iCAP, we then computed iCAP stability as the average cosine similarity between the cluster centroid (i.e., the global iCAP map) and the individual subject iCAP maps. We performed this analysis both considering healthy subjects and stroke participants together and separating the two groups. In order to better characterize the iCAPs spatial patterns and evaluate whether they were impacted by the presence of the stroke lesions, we computed the overlap between the locus of the lesion and the iCAPs maps. For this, we binarized the topography of the lesion using a threshold of $\frac{1}{4}$ of the maximum values of the summed binary masks over all 103 stroke patients (i.e., 25) and each iCAP map with a threshold of $Z = 1.5$ (i.e., same threshold of Fig. 2). We then calculated the dice coefficients for each iCAP map.

2.11.2. Group comparisons of iCAP spatial patterns

For each group and testing sessions, iCAP spatial patterns were obtained by averaging significant innovation frames belonging to the corresponding group and session. The group- and/or session-specific spatial patterns were then compared using dice coefficient. Spatial maps were thresholded with a threshold of $Z = 1.5$ (i.e., same threshold of Fig. 2) before computing the dice coefficients.

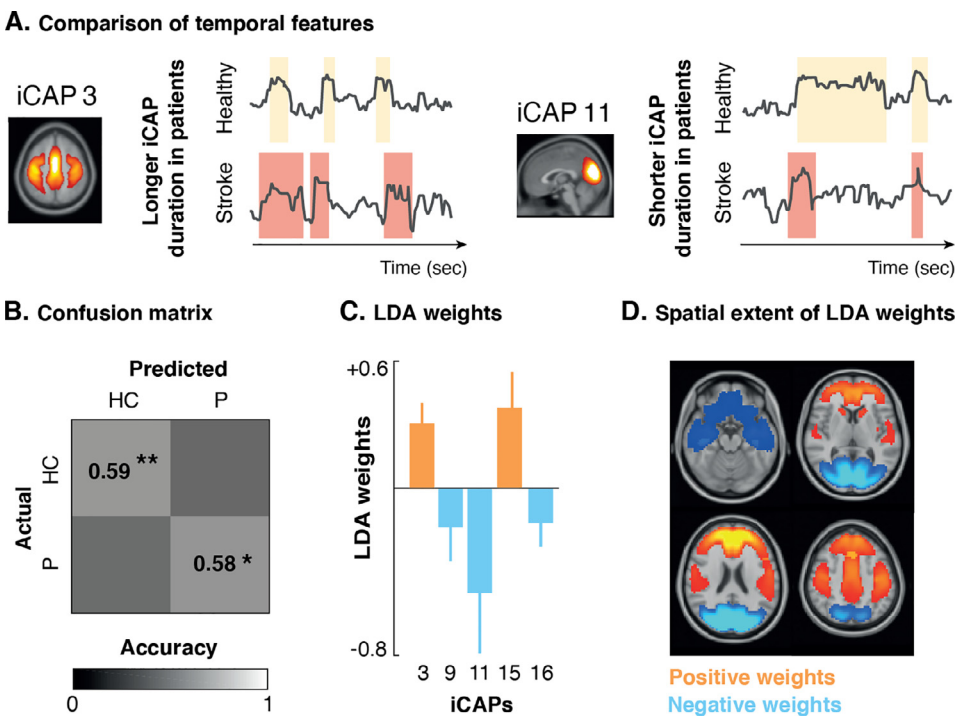

Fig. 3. Temporal features: comparison between healthy controls and patients | A. We used spatiotemporal transient-informed regression to derive iCAP time courses at the subject-level and to compute the average duration of each iCAP. Stroke patients showed a varied pattern of longer and shorter network activations when compared to healthy subjects. B. Confusion matrix for patients and healthy controls for the LDA classifier averaged over folds and groups (highest results obtained when considering 4 iCAPs). * $p < 0.05$; ** $p < 0.003$ (non-parametric permutation testing). C. LDA weights for the features that have been selected more than 50% over folds and subgroups (mean ± SD over folds and patients' subgroups). D. Linear combination of the features that have been selected more than 50% over folds and subgroups weighted by the LDA weights displayed in Montreal Neurological Institute coordinates. Blue represents locations with shorter duration for stroke patients; whereas orange represents locations with longer duration.

2.11.3. Stability of iCAP durations

Before investigating stroke-related changes in temporal dynamics of large-scale resting-state networks, we first evaluated the reliability of iCAP temporal properties in the control group. To this end, we assessed whether iCAP durations were stable within- and between-individuals in healthy subjects. Within-individuals stability was assessed by comparing the iCAP durations between the two sessions using a paired Wilcoxon signed rank test False Discovery Rate (FDR) corrected (Benjamini and Yekutieli, 2001). For the between-individuals comparison, instead, we randomly split the healthy subjects in two groups (ten different random splits were generated) and we compared, for each split, durations between the two groups using Wilcoxon ranksum test FDR corrected (Benjamini and Yekutieli, 2001). We performed this analysis both for time point 1 and time point 2.

2.11.4. Group comparisons of iCAP durations

In order to compare iCAP durations between patients and healthy control subjects, we deployed a multivariate analysis and specifically a Bayesian classifier, specifically a LDA (Fisher, 1936). Indeed, we hypothesized that the changes were not occurring in a single iCAP. We built a two-class LDA classifier (accounting for different covariance matrices for each class) using the durations of the 16 iCAPs. For this, because of the unbalance in number between healthy subjects and patients ($n = 38$ healthy subjects - 19 per session, and $n = 229$ patients - 103 for 1–2 weeks, 72 for 3 months, and 54 for one year) we split the dataset in 5 groups containing both sessions of the healthy subjects (i.e., in total 38 healthy subject observations) and all sessions of around 20 patients (i.e., in total around 45 ± 1 patient observations). We have performed an LDA analysis for each group separately. For each group, we then performed a cross-validation schema with 4 folds with both sessions of 5 healthy subjects (i.e., in total 10 healthy subject observations) and all sessions of around 5 patients (i.e., in total 11 ± 1 patient observations) per fold. For each fold, to rank the features of the classifier, we calculated the discrimination power for the two classes (i.e., patients and healthy controls) for each feature separately, using a two-sample Mann-Whitney test. Next, we ranked the features by their absolute standardized u-statistic obtained from this test. In the next stage, we sequentially added feature after feature and tested classification accuracy and area under the receiver operation characteristics (ROC) curve (AUC) in the left-out subjects (Pirondini et al., 2020). To further balance the two population groups, we have used a probability of 0.5 for each population group in the LDA classifier. Importantly, all the sessions of a subject were removed in the cross-validation schema. We averaged accuracy and AUC over folds and groups. Finally, in order to select the most discriminative features over folds and groups, we have counted how many times an iCAP was selected over folds and groups. We then considered as most discriminative features those that were selected at least 50% of the cases. To assess the statistical significance of the classification, for each group and fold, we built $N = 1000$ classifiers with randomly assigned labels at each permutation with the number of subjects matching the actual grouping. We then repeated the feature selection procedure used above calculating the discrimination power for the two random classes (i.e., patients and healthy controls) for each feature separately. Finally, we estimated AUC and classification accuracy for each permutation. For each repetition we averaged accuracy and AUC over folds and groups (i.e., random classification accuracy and AUC). For both measures, p-values were obtained as $1 - \sum_{i=1}^{N} \frac{p}{(N+1)}$ where p corresponds to the cases where the original AUC and/or classification accuracy are above random AUC and/or classification accuracy and N the total number of random classifiers (i.e., 1000).

2.11.5. Validation of LDA weights

In order to exclude that the changes in iCAPs duration between healthy subjects and patients were an artifact of the lesion, we evaluated the overlap between the LDA weights and the locus of the lesion. Specifically, we first obtained a linear combination of the features that were selected at least 50% over folds and subgroups (i.e., 5 most discriminative features) weighted by the LDA weights. We then binarized this map using a threshold of -/+ 0.5 (i.e., same threshold used in Fig. 3) and computed the dice coefficient between this binarized map and a binarized topography of the lesion. The topography of the lesion was obtained using a threshold of $\frac{1}{4}$ of the maximum values of the summed binary masks over all 103 stroke patients (i.e., maximum value = 25).

2.11.6. Partial least squares correlation

We deployed partial least squares correlation (PLSC) (Zöller et al., 2019; Zöller et al., 2017; D. Zöller et al., 2018; Kebets et al., 2019; Delavari et al., 2021) to evaluate multivariate patterns of correlation

between iCAP durations and: (i) white matter disconnections; (ii) behavioral scores and recovery.

PLSC has been previously successfully employed to characterize covarying patterns of structural and functional connectivity in healthy individuals, and it is nowadays considered a clinically relevant method (Zöller et al., 2019; Zöller et al., 2017; D. Zöller et al., 2018; Kebets et al., 2019; Delavari et al., 2021; Krishnan et al., 2011). It seeks to define linear combinations of two data matrices (**X**, i.e., the brain networks properties – iCAP durations, and **Y,** i.e., the anatomical (i) or behavioral variables (ii)) that maximally explain the covariance between the two matrices. The first step in PLSC is the computation of the correlation matrix between **X** and **Y** (***R* = X'Y**). In our approach, **X** and **Y** were z-scored across subjects before correlation. Then **R** is decomposed in *N* latent variables, or "correlation components" (where *N* is the minimum number between the number of included behavioral/anatomical variables and the number of iCAPs), using singular value decomposition ***R*=USV'** with **U'U=V'V=*I***. Each correlation component has a singular value (on the diagonal of **S**) that specifies the explained correlation, as well as *Nx* iCAP durations saliences or "duration weights" (rows of **V'**) and *Ny* behavioral/anatomical saliences or "behavioral/anatomical weights" (columns of **U**). The saliences (which lie between −1 and 1) indicate how strongly each variable contributes to the multivariate behavioral-brain/anatomical-brain correlation in a certain correlation component. We used permutation testing with 1000 permutations to evaluate if any of the correlation components was significant and bootstrapping with 500 bootstrap samples with replacement to evaluate the stability of the behavior/anatomical and brain weights. Brain and behavioral/anatomical saliences were recalculated for every bootstrap sample, resulting in a typical bootstrap distributing of the salience values. Saliences were considered significant if lower/higher than lower/upper bound of 95% confidence interval of bootstrapping distributions.

Here below more details about the two PLSC analysis performed in this study:

1 we conducted a PLSC analysis with duration of the 16 iCAPs as brain variables and with white matter tract disconnections as anatomical variables. We considered in the PLSC both patients with severe acute deficits (i.e., > 2 SD from healthy subjects at 1–2 weeks post-lesion) and patients with less severe acute deficits (i.e., < 2 SD from healthy subjects) without distinction. We computed a PLSC for all the three time points separately (i.e., 1–2 weeks; 3 months; 1-year post-lesion). PLSC analysis p-values were corrected for multiple comparisons across the three time points domain using FDR at $q<0.05$ (Benjamini and Yekutieli, 2001). Because of the difference in number of patients between the three time points ($n = 103$ for 1–2 weeks, $n = 72$ for 3 months, and $n = 54$ for 1-year post-lesion), we assessed whether the significance in the PLSC was influenced by the number of patients. Specifically, we repeated the PLSC between white matter tract disconnections and iCAPs duration for 1–2 weeks post-lesion with 100 groups of 72 (i.e., number of patients at 3 months) randomly selected patients and 100 groups of 54 (i.e., number of patients at 1-year) randomly selected patients and we checked the significance of the PLSC for each group.
2 Because patients with/without severe acute deficits showed different recovery trajectories over time (see **Figure S1** and (Ramsey et al., 2017)), we computed a group PLSC analysis between the 16 iCAP durations and the behavioral scores for three groups: patients without severe acute deficits, patients with severe acute deficits, and healthy controls as normative data. Group PLSC analysis entails that a correlation matrix is computed per group (in this case healthy controls $\mathbf{R_{HC}}$, patients with less severe acute deficits $\mathbf{R_{ND}}$, and patients with severe acute deficits $\mathbf{R_D}$). The common correlation matrix R is then computed by concatenating $\mathbf{R_{HC}}$, $\mathbf{R_{ND}}$ and $\mathbf{R_D}$ resulting in 3*Ny* behavior saliences. We can then compute the so called "brain scores" by projecting every individual's iCAP durations onto the respective brain weights with **Lx=XV**. PLSC analysis was computed for each neuropsychological domain (attention, spatial memory, verbal memory, language, and motor) separately, as only a limited number of participants performed the assessment for all four classes (**Table S1**). In order to capture multivariate patterns of correlation with the behavioral measures and the recovery, we have used an innovative way of coding the design matrix for the behavioral scores (Delavari et al., 2021) that includes two behavioral variables: the mean behavior in subjects, and the delta behavior in subjects (see Fig. 5A for a schema of the PLSC). The former assigned the mean value of the first PCA component of a subject across all visits for each time point. The latter corresponded to the difference between the actual value of the first PCA component of a subject at a time point and the subject's mean value of the first PCA component. It is worth noting that, by construction, mean behavior and delta behavior are orthogonalized and can be interpreted as the cross-sectional and longitudinal effect of behavior, respectively. We then defined "inter behavior" as the interaction between mean behavior and delta behavior, which enables the capture of concave or convex (i.e., U-shaped) recovery trajectories that we hypothesized to be different between patients with and without severe acute deficits (see **Figure S1** and (Ramsey et al., 2017)). This design matrix allows us to correctly capture the within- and between-subject effect of recovery highlighting these different trajectories. PLSC analysis p-values were corrected for multiple comparisons across behavioral domain using FDR at $q<0.05$ (Benjamini and Yekutieli, 2001).

3. Results

3.1. Lesion topography and behavioral profile of patients

We studied a large population of stroke patients and age-matched healthy subjects (i.e., in total 267 acquisitions, **Table S1**) that was partially presented in previous publications (Siegel et al., 2016; Salvalaggio et al., 2020; Siegel et al., 2018; Griffis et al., 2020; Griffis et al., 2019; Corbetta et al., 2015; Ramsey et al., 2017). Briefly, first-time stroke patients with clinical evidence of impairment were recorded longitudinally: 1–2 weeks ($n = 103$), 3 months ($n = 72$), and 12 months ($n = 54$) after the lesion. The healthy control group ($n = 19$) also underwent two imaging sessions at a distance of 3 months. Lesion volume varied greatly over patients (ranging from 0.1 cm^3 to 277.02 cm^3, mean ± SD volume: 33.66 cm^3 ± 49.51 cm^3), with the highest overlap found in white matter and subcortical regions (**Figure S1a**). Specifically, the most affected tracts were the corticospinal tract, the fronto- and parieto-pontine tract, the extreme Capsule (EMC), and the inferior fronto-occipital fasciculus (IFOF) (**Figure S1b-c**). Prior to each fMRI scan, patients were tested with an exhaustive neurobehavioral battery. We applied principal component analysis (PCA) on these behavioral data to isolate clusters of deficits for each domain separately (e.g., motor, language, attention, spatial memory, and verbal memory) (Corbetta et al., 2015). We found factors analogous to our previous works (see *Behavioral domain scores* section (Corbetta et al., 2015; Ramsey et al., 2017)) and also similar recovery effects (Corbetta et al., 2015; Ramsey et al., 2017). Indeed, patients with severe acute deficits (i.e., > 2 SD from healthy subjects at 1–2 weeks post-lesion) got closer to the healthy subjects within the first three months post-lesion (Figure S1d). Instead, patients with less severe acute deficits (i.e., < 2 SD from healthy subjects) had stable performances over sessions comparable to those of the healthy subjects. Importantly, the global variance over subjects was found to decrease over time points, suggesting that the outlier population defined at the first time point reflects actual deficits in the acute state, rather than random error in the behavioral indicators. Moreover, this observation indicates that subsequent changes are primarily driven by neurological recovery and not by a mere regression to the mean of outlying values defined at the first time point.

Whole brain dynamics is preserved in patients

We applied Total Activation on the denoised BOLD time courses to retrieve robust transient activity (i.e., frames with highly changing activity, the so-called significant innovation frames), individually for the 267 acquisitions considered (**Fig. 1**). Patients and healthy subjects had a comparable number of transients considering both positive and negative frames (i.e., time points with jointly activating - positive frames - and jointly deactivating - negative frames - regions; mean ± SD - healthy controls: 43.8 ± 12.0; patients 1–2 weeks: 45.8 ± 22.4; 3 months: 43.4 ± 19.5; 1 year: 43.7 ± 20.4, expressed in percentage of the total number of frames for each subject - **Fig. 2a**), highlighting that the whole brain overall amount of dynamic fluctuations was preserved after stroke. Yet, dynamics of specific brain regions could still be affected by the lesion. For this reason, we then extracted spatial patterns of large-scale networks and we computed dynamic features for each network individually.

Resting-state activity can be decomposed into spatial maps corresponding to known functional networks

Transients of both healthy subjects and patients at different time points were fed to a k-means clustering to obtain stable innovation-driven co-activation patterns (iCAPs), which could be spatially and temporally overlapping. The number of clusters was determined using evidence accumulation and, as a result, 16 iCAPs were extracted (**Figure S2a**). The iCAPs corresponded to well-known resting-state networks obtained with other approaches (Van Den Heuvel and Pol, 2010; Lee et al., 2013), in line with our previous results in different datasets (**Fig. 2b** and **Table S2**) (Karahanoğlu and Van De Ville, 2015; A. Tarun et al., 2020; Zöller et al., 2019; Piguet et al., 2021). Importantly, the spatial profile of the iCAPs did not appear to be influenced by the presence of the lesions, as demonstrated by a minimal overlap between the lesion locus and the iCAPs maps ([0 0.05] range of dice coefficients over iCAPs). Specifically, the iCAPs included sensory-related networks such as primary and secondary visual areas (iCAP 6), auditory and language network (iCAP 5), with high activations in Heschl gyrus and rolandic operculum, and sensorimotor network (iCAPs 3 and 8), which included pre-, post-, and paracentral areas, supplementary motor area, and middle cingulum (only for iCAP 3). Two iCAPs ((Fox et al., 2005) and (Bullmore and Sporns, 2009)) represented the visuospatial/ventral attention network and comprised the primary (iCAP 1) and secondary (iCAP 11) visual areas along with the precuneus. There was an additional task-related iCAP, the fronto-parietal network (iCAP 4), with high activations in the frontal and parietal lobes together with anterior and middle cingulate cortex (ACC and MCC). As previously reported (Karahanoğlu and Van De Ville, 2015; A. Tarun et al., 2020; Zöller et al., 2019), the Default Mode Network (DMN) was decomposed into a frontal part (iCAP 12) including frontal lobe and ACC, and a posterior part (iCAP 10) comprising the cuneus, the precuneus, and the superior and inferior parietal lobes. Four iCAPs included regions of the cerebellum (iCAPs 2, 7, 13, and 16). Yet, iCAPs 13 and 16 were specific to the anterior (iCAP 13) and posterior cerebellum (iCAP 16); whereas iCAP 2 included as well secondary visual areas and iCAP 7 hippocampal areas. The remaining iCAPs comprised regions of the salience network, with iCAP 15 encompassing middle and superior frontal lobe and ACC, and iCAP 9 related to the inferior temporal lobe, the hippocampus and the amygdala.

iCAP spatial maps are similar between patients and controls

Prior to evaluating differences between patients and healthy controls, we first assessed between-session spatial replicability of the iCAPs in healthy subjects. The high similarity of the spatial patterns (mean dice coefficients over iCAPs ± SD: 0.85 ± 0.04 **Figure S3a**) emphasized the ability of the iCAP framework to extract reliable and stable networks. Interestingly, spatial maps were also very similar between patients and healthy controls (mean dice coefficients over iCAPs ± SD at 2 weeks: 0.87 ± 0.03; 3 months: 0.88 ± 0.03; 1 year: 0.88 ± 0.04 - **Fig. 2c** and **Figure S3b**), as previously reported using static functional connectivity (Siegel et al., 2016). Finally, spatial maps were also highly comparable between left and right damage patients (mean dice coefficients over iCAPs ± SD: 0.90 ± 0.04 **Figure S3c**).

Patients exhibited a varied pattern of longer and shorter resting-state network activations

The stability of the spatial maps over sessions (**Figure S3a-c**) and groups (**Fig. 2c**) highlighted the robustness of the brain's functional architecture, as described using iCAPs. We capitalized on this observation to investigate the temporal properties associated with these large-scale brain networks. To this end, we used spatiotemporal transient-informed regression to derive iCAP time courses at the subject-level and to compute the average duration of each iCAP (**Fig. 1**). Similarly to our assessment of spatial replicability, we evaluated the within- and between-individual temporal replicability in the healthy subjects. Given the stability of average iCAP durations in the healthy control group ($p >$ 0.31 - FDR corrected (Robb and Hanson, 1991) for the within-subjects comparison, see **Figure S3ed**; and $p > 0.15$ - FDR corrected (Robb and Hanson, 1991) for the between-subjects comparison), we then probed whether this temporal measure could be leveraged as a discriminative feature to distinguish stroke patients and healthy subjects (**Fig. 3a**). Considering that patients present with a combination of deficits in different domains, which may reflect dysfunction across multiple brain networks (Carter et al., 2012), we opted for a multivariate approach, which considers a combination of multiple features instead of individual networks (Haller et al., 2014). Indeed, we hypothesized that the changes were not occurring in a single iCAP, but over a set of iCAPs, as further demonstrated from the correlation with the behavioral deficits. We performed a Linear Discriminant Analysis (LDA) with a cross-validation scheme (Fisher, 1936) that allowed to discriminate between the two groups with a significant accuracy (0.58 - $p < 0.004$), as illustrated by a diagonal confusion matrix (**Fig. 3b**), and sensitivity-specificity, as emphasized by the area-under the curve (AUC: 0.58 - $p < 0.004$). 5 features were stable over patients' subgroups and folds (i.e., features present more than 50% of the cases) and captured specific regions whose temporal profiles were affected in stroke patients. In particular, patients showed a longer duration in pre-central areas and in the anterior and medium cingulum. Instead, the occipital lobe and the postero-lateral cerebellum had a reduced duration (**Fig. 3c-d**). A similar varied pattern of longer and shorter network activations was observed when looking at individual iCAP durations of healthy controls and stroke patients at different points in time after lesion (**Figure S3f**). Additionally, the discriminatory weights had a minimum overlap with the locus of the lesion (dice coefficient = 0.02), emphasizing that the changes in iCAPs duration were not an artifact of the lesion.

Changes in duration are explained by disconnections within white-matter tracts

In order to better understand the interplay between functional dynamics and anatomy, we deployed a partial least square correlation (PLSC) analysis between iCAP average durations and disconnections within white-matter tracts (**Fig. 4a**). We found a single significant component (p-value = 0.017 - FDR corrected; $\rho = 0.35$), only for patients at 1–2 weeks post-lesion. Importantly this was not explained by the higher number of patients at 1–2weeks post-lesion as compared to the other time points (the significance held also with a reduced number of subjects – 72 or 54 – in 81.5 ± 9.2% of the cases). Microstructural changes in the weeks/months following the stroke can be reasonably expected because of inflammatory reactions as well as degenerative and neuroplastic processes, leading to further changes in the anatomical disconnections. However, white matter disconnections were obtained only from structural images obtained at 1–2 weeks post-lesion and this could explain why the PLSC were significant only for this time point. The longer duration of the iCAPs (**Fig. 4b left panel**) was explained by the loss of white matter fibers (**Fig. 4b right panel**), in particular of *i)* the projection pathways, which connect cortical areas with subcortical nuclei and brainstem; *ii)* a few association pathways which connect disparate cortical areas including the cingulum, the EMC, the IFOF, and the uncinate fasciculus; *iii)* the anterior and middle commissure; and *iv)* the fiber bundles inside the brainstem (i.e., the medial lemniscus and the spinothalamic tract). Interestingly, the fiber bundles in the cerebellar

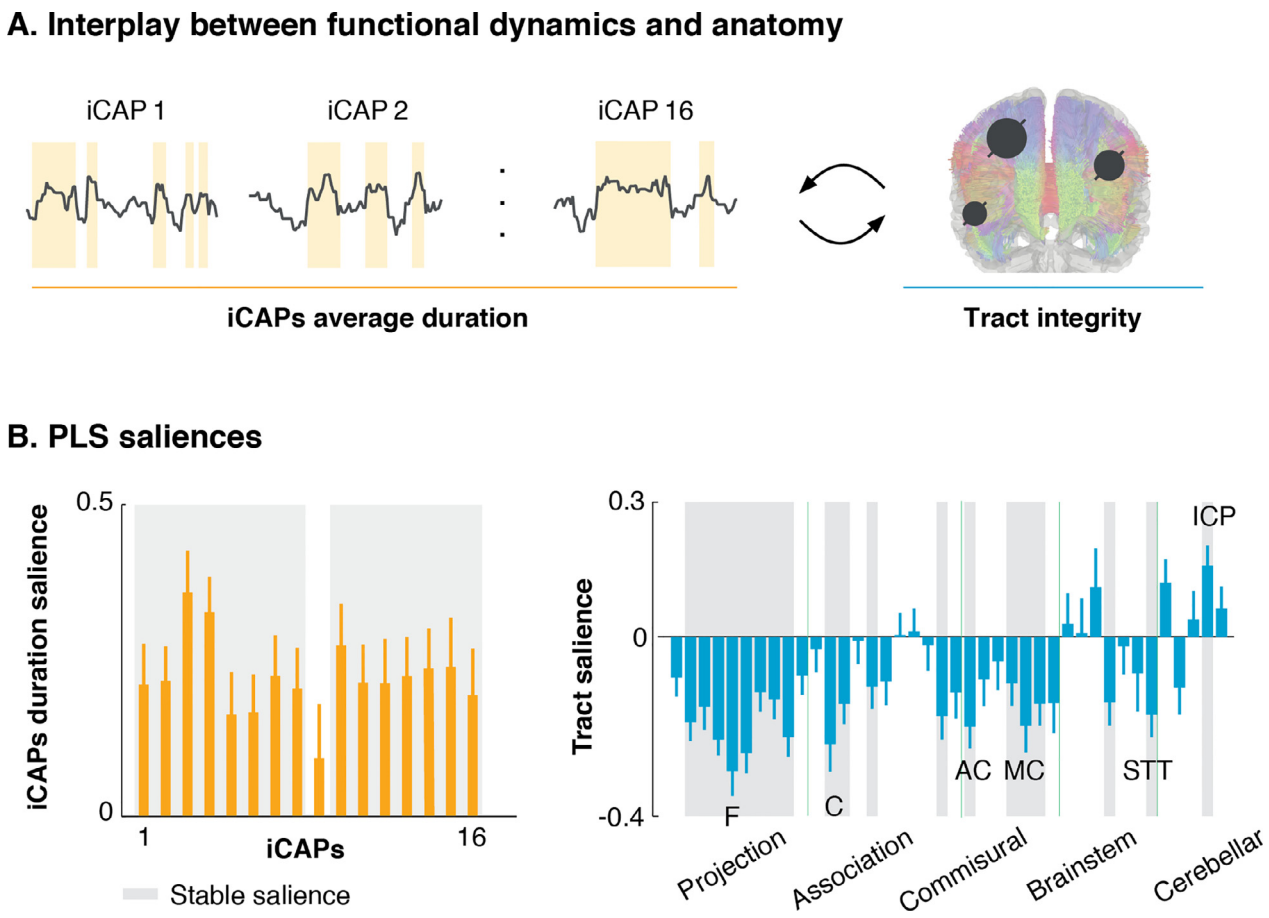

Fig. 4. Interplay between functional dynamics and disconnection within white-matter tracts | A. We deployed a PLSC analysis between iCAP average durations and disconnections within tracts for patients at 2 weeks post-lesion (Griffis et al., 2020; Griffis et al., 2019). B. Left panel: iCAP durations saliences for the significant PLS component (p = 0.003) (mean ± SD over bootstrap repetitions); Right panel: disconnections within tracts saliences of the significant PLS component (mean ± SD over bootstrap repetitions). Tracts were grouped in projection pathways, association pathways, commissural pathways, brainstem pathways, and cerebellar pathways following (Yeh et al., 2018). GG Gray shadows indicate stable salience, i.e., saliences lower/higher than the lower/upper bound of 95% confidence interval of bootstrapping distributions (bootstrapping procedure with 500 random samples with replacement). F: fornix; C: cingulum; AC: anterior commissure; MC: medial commissure; STT: spinothalamic tract; ICP: inferior cerebellar peduncle.

pathways, and specifically the inferior cerebellar peduncle had opposite saliences (i.e., positive saliences) highlighting a different behavior for the cerebellar structure, characterized by a lower average duration as compared to healthy controls.

Changes in duration are associated with behavioral deficits and recovery

We then assessed whether changes in iCAP durations correlated with clinical impairments and recovery, as estimated using the behavioral measures. We applied a second PLSC analysis, this time between the temporal measures and the behavioral data of the three time points, separately for each domain (**Fig. 5a**). Functional network durations showed significant correlations with recovery from attention, language, and spatial memory deficits (attention: p-value adjusted for multiple comparisons = 0.05, ρ = 0.23; language: p-value = 0.015, ρ = 0.18; spatial memory: p-value = 0.018, ρ = 0.18), but not from motor or verbal memory impairments (p-value adjusted > 0.06). This observation parallels our previous findings regarding the relationship between brain modularity and behavior, in which a reduction in modularity was observed in the sub-acute stage, followed by a partial recovery, limited to attention, language and spatial memory (Siegel et al., 2018). To further explore the clinical relevance of our results, we first investigated the saliences related to the behavioral data. We observed that they were only significant for patients with severe acute deficits, which were the ones showing the largest recovery over time (**Figure S1d**). We then investigated the saliences pertaining to iCAP durations and highlighted that temporal patterns were behavior-specific (mean correlation ± SD over behaviors: 0.22 ± 0.08, **Fig. 5b**). Indeed, attention domain had saliences in the fronto-parietal network, the amygdala, the precuneus and the visual cortex (**Fig. 5c**). Spatial memory symptoms, instead, were mostly correlating with fronto-parietal and sensorimotor networks, the posterior part of the cerebellum, the amygdala, and the visual cortex. Finally, language-related deficits were specifically tied to the language network and primary and secondary visual areas. In order to probe the temporal evolution of these brain functional components, we then projected the individual subject's iCAP durations onto the significant multivariate brain saliences for healthy controls and for patients with severe acute deficits (**Fig. 5d**). Intuitively the brain scores show how the iCAPs duration changes over time. Specifically, over time, the brain scores of stroke patients approached those of healthy controls (absolute distance between patients and healthy subjects at 1–2 weeks: 0.37, 1.80, and 1.94 for language, attention, and spatial memory respectively; at 1-year post-lesion: 0.07, 1.37, and 0.94), suggesting that post-stroke network dynamics restored proportionally to behavioral improvement.

4. Discussion

In recent years, *dynamic* functional connectivity methods have been demonstrated to provide additional insights into the rich spatiotemporal orchestration of spontaneous fluctuations as compared to *static*

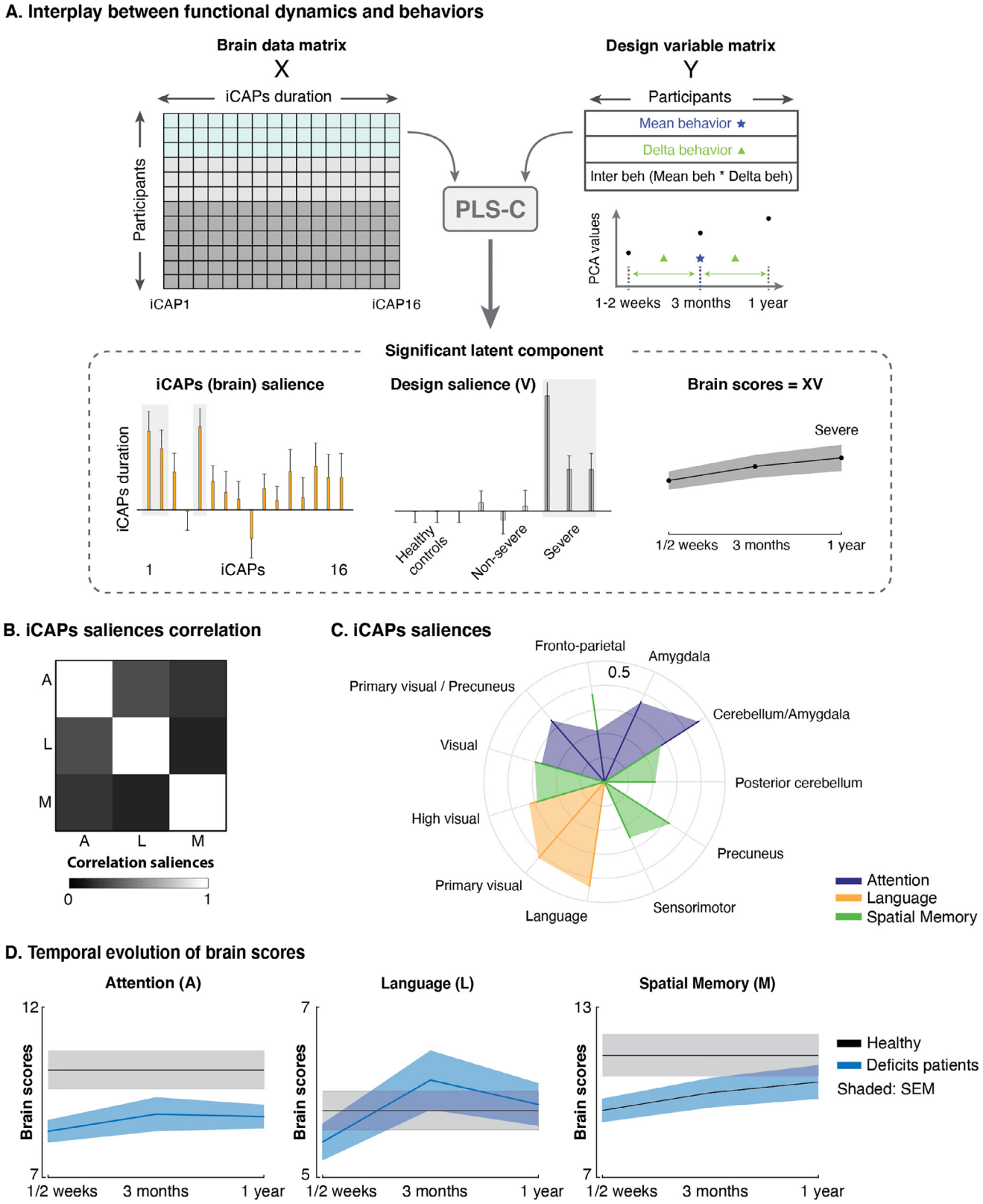

Fig. 5. Interplay between functional dynamics and behavioral deficits | A. We deployed a PLSC analysis between iCAP average durations and behavioral scores and recovery for all patients and all sessions. B. Correlation matrix between iCAP durations saliences between the three behavior domains that had one significant PLS component (i.e., attention, language, and spatial memory). C. iCAP durations saliences for attention (blue), language (orange), and spatial memory (green). D. Brain scores obtained projecting the individual subject's iCAP durations onto the significant (i.e., saliences lower/higher than the lower/upper bound of 95% confidence interval of bootstrapping distributions, which were determined by bootstrapping procedure with 500 random samples with replacement) multivariate brain saliences (i.e., Lx=XV, see Methods) for healthy controls (black) and for patients with severe acute deficits (blue) for the three behavior domains and the three time points (i.e., 1–2 weeks, 3 months, and 1-year post-lesion) separately. Shadows represent SEM.

approaches (Preti et al., 2017; Cohen, 2018; Karahanoğlu and Van De Ville, 2017; Hutchison et al., 2013), in particular for psychiatric conditions (Bolton et al., 2020). However, the transition towards dFC in the context of stroke has so far remained limited (Bonkhoff et al., 2020; A.K. Bonkhoff et al., 2021; A.K. Bonkhoff et al., 2021; Hu et al., 2018; Obando et al., 2019; Duncan and Small, 2018; Chen et al., 2018). While these studies nicely highlighted the advantage to use dFC to better capture reorganization of brain networks following stroke, they suffer from three main drawbacks: small sample sizes, major focus on motor deficits, and investigations limited to slow dynamical changes (sliding window approaches). Here we extended these results by applying a state-of-the-art data-driven dynamic method, the iCAP framework in an extensive cohort of stroke patients ($n = 103$) with heterogeneous neurological syndromes and scanned longitudinally (Siegel et al., 2016; Salvalaggio et al., 2020; Siegel et al., 2018; Griffis et al., 2020; Griffis et al., 2019; Corbetta et al., 2015; Ramsey et al., 2017). We uncovered a temporal imbalance of network recruitment compared to healthy controls and showed how these dynamic changes articulate with anatomical and behavioral disruptions.

Delving into network dynamics

We deployed the iCAP framework and found sixteen large-scale brain networks, or iCAPs, whose spatial patterns agreed with previous literature using the iCAP framework (Karahanoğlu and Van De Ville, 2015; A. Tarun et al., 2020; Zöller et al., 2019; Piguet et al., 2021) as well as other statistical approaches (Van Den Heuvel and Pol, 2010; Lee et al., 2013). Importantly, this spatial organization was robust over sessions in healthy subjects and had similar patterns in participants with stroke. In particular, networks were bilateral regardless of the side of the lesion, suggesting a preserved organization across brain regions. While this might seem in contradiction with the decrease in interhemispheric connectivity previously reported post-stroke (Siegel et al., 2016; Griffis et al., 2019; Carter et al., 2010), it should be noted that fine-grained coordination between brain areas can be occulted when using classical *static* FC approaches (Bonkhoff et al., 2020; A. Tarun et al., 2020). For instance, the correlation between distinct brain areas exhibiting both positive and negative correlations in distinct time-windows would result in a low *static* functional connectivity, in spite of the dynamic synchronization existing between these regions (A. Tarun et al., 2020). Therefore, it follows that a decrease in FC does not necessarily imply a decrease in global network activity. However, decreased FC might reflect an overall reduction in the efficiency of information transfer, which could manifest in the form of aberrant durations of functional networks (Bullmore and Sporns, 2009; Zöller et al., 2019; Siegel et al., 2018).

To evaluate these time-varying properties, we thus derived subject-specific iCAP time-courses and computed average durations of activation for each individual iCAP, a measure that cannot be explained in terms of *static* connectivity. Of note, a similar approach previously allowed to show the link between brain dynamics and risk factors for schizophrenia in 22q11.2 deletion syndrome (Zöller et al., 2019). Here we first demonstrated that network durations were robust between- and within-individuals in healthy subjects highlighting the applicability of our method for clinical explorations. Importantly, our results were stable despite the small sample size of the control group, which yet was comparable to several previous works (Karahanoğlu and Van De Ville, 2015; Kinany et al., 2020). In contrast, durations were affected post-stroke. Specifically, patients exhibited a varied pattern of longer and shorter network activations alluding to an “under-engagement” in certain brain states coupled with an “over-engagement” in others. These results, combined with the preserved overall amount of dynamic fluctuations (i.e., similar number of significant innovation frames between patients and healthy subjects), hint at a dynamical imbalance following stroke, rather than an overall shift towards a slower or a faster brain activity. A compelling observation was that networks usually associated in static analyses, such as the two sensorimotor networks (iCAPs 3 and 8) presented opposite engaging behaviors after lesions (see **Fig. 3** and **Figure S3f**). This suggests that intricate and non-stationary behavior are also present within overlapping brain regions, something that would be overlooked when relying on conventional *static* methods.

Structural substrates of disrupted dynamics

We then assessed whether this post-stroke imbalance was determined by structural damages. Indeed, white matter connections, when intact, form the anatomical scaffold that mediates the dynamic fluctuations between networks (A. Tarun et al., 2020; Calamante et al., 2017; Nozais et al., 2021). As such, interruptions in these connections may impact the brain’s functional organization, not only in the vicinity of the lesion, but also on a larger scale. In particular, disruption of white matter connections might affect the flow of information exchange between distant brain regions, thus altering the dynamics of network transitions and consequently their temporal characteristics. However, understanding how the human brain orchestrates large-scale functional networks despite being constrained by a rigid anatomical substrate and how this orchestration is affected by lesions is still an open question in clinical neuroscience (Zoeller et al., 2019; Muldoon et al., 2016). Here, we explored this relationship by probing how iCAP temporal properties varied with structural measures of disconnections (Griffis et al., 2020; Griffis et al., 2019) and we found that altered durations were explained by the disruption of white matter tracts, particularly within the projection pathways, as well as within the cingulum and the commissural pathways. Specifically, the projection pathways subserve the subcortical integration of sensorimotor inputs and outputs between the cerebral cortex and the peripheral system. The commissural pathways, instead, connect cerebral hemispheres. Both these pathways are involved in providing local and global efficiency (Yeh et al., 2018), measures that are indicative of the capacity for parallel information transfer and integrated processing between, respectively, short- and long-distance regions (Bullmore and Sporns, 2009). As such, disruptions of these tracts likely drive the widespread neurobiological processes occurring in the course of stroke recovery (Siegel et al., 2018).

Domain-specific behavioral correlates

Finally, we assessed whether these lesion-induced changes in network dynamics correlate with behavioral impairments and recovery. To this end, we capitalized on the longitudinal nature of the dataset so as to assess short- and long-term recovery processes and on its multi-domain clinical assessments. Earlier observations indicated that most deficits restore within three months, with additional recovery, yet more limited, up to one year following lesion (Ramsey et al., 2017). Interestingly, these multi-scale recovery patterns were reflected in the temporal dynamics of brain activity, as the initial imbalance observed in severely affected patients normalized towards the level of healthy subjects, mostly within the first three months. Thanks to the heterogeneous patient population, we showed that these trends were significant only for attention, language and spatial memory disorders, as also observed for post-stroke decrease in network modularity in an earlier study (Siegel et al., 2018). This suggests that both modularity and network duration are associated with higher cognitive deficits, in the form of functional changes likely reflecting inter-hemispheric homotopic integration and within-hemisphere segregation (Siegel et al., 2016). It is noteworthy that these alterations in static connectivity were not reflected in the spatial organization of the large-scale networks but on their temporal durations. Importantly, recovery of motor and verbal memory deficits did not correlate with changes in iCAPs duration. It should be noted that these results may be partially impacted by the choice of the threshold employed to divide patients without and with severe deficits (i.e., > 2 SD from healthy subjects in the subacute phase). Additionally, while changes in the population variance over time suggest that longitudinal improvements in behavioral scores are primarily driven by neurological recovery, we cannot rule out the possibility that the variance at the first time point might reflect a combination of genuine deficits, baseline interindividual variability, and random error, in which case subsequent measurements would show partial regression to the mean. This should be considered when interpreting our results. However, while other thresholds could be

explored, this choice was consistent with our previous works (Siegel et al., 2016; Siegel et al., 2018; Corbetta et al., 2015; Ramsey et al., 2017). Importantly, this allowed direct comparison, and emphasized that the current these results parallel our previous findings in brain modularity changes (Siegel et al., 2018). Interestingly, they seem at first to contradict recent works showing that dynamic connectivity-derived parameters predict motor acute impairment and recovery (Bonkhoff et al., 2020; A.K. Bonkhoff et al., 2021; A.K. Bonkhoff et al., 2021). However, this correlation seems to be limited to the sensorimotor networks and not to large-scale brain networks, which might hinder the correlation with the motor deficits. Indeed, motor deficits are known to be better predicted by lesion location (Siegel et al., 2016) and to changes in the sensorimotor networks directly affected by the lesion, probably indicating that these functions rely less on information integration between large-scale networks. Complex cognitive functions (such as attention, memory, and spatial memory), instead, are generated by integrations of inputs between different brain areas and so are probably more affected by widespread changes in functional connectivity (*connectional diaschisis*). Further supporting this differential nature of impairments, changes in duration were network-specific (e.g., only durations of auditory and visual networks correlated with language deficits). Finally, deficits and recovery were associated with distant brain regions, bringing new evidence to corroborate that stroke is not a focal disease but, instead, a network disease (Carrera and Tononi, 2014; Allali et al., 2018).

Clinical considerations

In summary, we found that durations of large-scale resting-state networks were altered as a consequence of interruptions in white-matter tracts. The brain was, therefore, less resilient and modular after stroke, as previously hypothesized (Siegel et al., 2018). Importantly, the restoration of the networks' natural temporal properties, likely accompanied by a restoration of this resilience, was crucial to achieve behavioral recovery, especially for cognitive deficits. Altogether, these results underscore the clinical relevance of network temporal properties, in particular as regards their duration. Therefore, dynamic functional connectivity methods seem crucial to inform the therapeutic process in several ways. First of all, as demonstrated here, they could elucidate pathophysiology changes post-stroke informing whether the rehabilitation-mediated changes may be going in the right directions, approaching the brain functional organization observed in healthy subjects, or may be maladaptive. Second, they could be used to predict the patients' outcome. In this regard, a recent work from Bonkhoff and colleagues (A.K. Bonkhoff et al., 2021) demonstrated for the first time that dynamic connectivity-derived parameters outperform static connectivity measures in the prediction of acute impairment and recovery. Yet new works are now necessary to probe whether the iCAP durations can predict the patients' recovery. Finally, these time-resolved methods could capture potential therapeutic targets that could possibly be modulated, for instance using non-invasive brain stimulation. While such interventions have been frequently employed to improve motor recovery after stroke (Guggisberg et al., 2019; Coscia et al., 2019; Koch and Hummel, 2017), only a restricted number of attempts have explored brain stimulation to treat post-stroke cognitive deficits (Yin et al., 2020), despite several successful applications in psychiatry (Drysdale et al., 2017). In this field, recent investigations jointly considering anatomy and functional dynamics provided valuable insights to guide neuromodulation treatments (Muldoon et al., 2016; Khambhati et al., 2019). In this regard, we foresee that investigating stroke-related disruptions using dynamic approaches could help shed light on meaningful temporal properties, which are directly tied to the underlying anatomical substrate, and that can be more readily leveraged to tune neuromodulation parameters. Considering that brain stimulation approaches can change excitability of functional connections within and between cortical areas with a high temporal and topographical resolution (Guggisberg et al., 2019), tuning parameters based on temporal properties could enable a better modulation of large-scale brain networks with the aim to improve a patient's clinical outcome. For instance, iCAP information could be used as a marker to guide neuromodulation protocols such as transcranial magnetic stimulation (TMS). The advent of multimodal recording and stimulation techniques such as TMS-fMRI is making this possible (Beynel et al., 2020). Yet this application still requires several steps including demonstrating that iCAP durations can be modified by TMS stimulation. However, only the use of dynamic methods enabling the study of the time-varying properties of brain networks can open such possibilities. Importantly for this, it is noteworthy that dFC methods do not require additional acquisition constraints for the patients. As such, clinical transitions to fMRI time-resolved methods appear not only necessary but also technologically possible.

5. Author contributions

Elvira Pirondini: Conceptualization, Methodology, Software, Formal analysis, Writing – Original Draft, Visualization; **Nawal Kinany:** Conceptualization, Methodology, Software, Formal analysis, Writing – Original Draft, Visualization; **Cécile Le Sueur:** Formal analysis, Writing - Review & Editing; **Joseph C. Griffis:** Formal analysis, Writing - Review & Editing; **Gordon L. Shulman:** Investigation, Data Curation, Writing - Review & Editing; **Maurizio Corbetta:** Investigation, Data Curation, Writing - Review & Editing, Supervision; **Dimitri Van De Ville**: Conceptualization, Methodology, Writing – Original Draft, Supervision.

Declaration of competing Interests

The authors declare no competing interests.

Data and script availability

Further information and requests for resources (e.g., specific codes and processed data) should be directed to and will be fulfilled by the Lead Contacts, Drs. Elvira Pirondini and Dimitri Van de Ville. The full set of neuroimaging data (along with behavioral data) are available at http://cnda.wustl.edu/app/template/Login. Matlab code for the application of the iCAP framework can be found at https://www.c4science.ch/source/iCAPs. Matlab code for the application of the PLSC analysis can be found at https://github.com/danizoeller/myPLS.

Acknowledgments

The authors would like to thank Drs. Anjali Tarun and Daniela Zöller for the inspiring discussions and Drs. Giulia Preti and Raphaël Liégeois for their comments on the manuscript.

Supplementary materials

Supplementary material associated with this article can be found, in the online version, at doi:10.1016/j.neuroimage.2022.119201.

References

Allali, G., et al., 2018. Brain imaging of locomotion in neurological conditions. Neurophysiol. Clin. 48, 337–359.

Andersson, J.L., Jenkinson, M., Smith, S., 2007. In: Non-Linear Registration, Aka Spatial Normalisation FMRIB Technical Report TR07JA2, 2. FMRIB Analysis Group of the University of Oxford, p. e21.

Benjamini, Y., Yekutieli, D., 2001. The control of the false discovery rate in multiple testing under dependency. Ann. Stat. 1165–1188.

Beynel, L., Powers, J.P., Appelbaum, L.G., 2020. Effects of repetitive transcranial magnetic stimulation on resting-state connectivity: a systematic review. Neuroimage 211, 116596.

Bolton, T.A., Morgenroth, E., Preti, M.G., Van De Ville, D., 2020. Tapping into multi-faceted human behavior and psychopathology using fMRI brain dynamics. Trends Neurosci..

Bonkhoff, A.K., et al., 2020. Acute ischaemic stroke alters the brain's preference for distinct dynamic connectivity states. Brain 143, 1525–1540.

Bonkhoff, A.K., et al., 2021a. Abnormal dynamic functional connectivity is linked to recovery after acute ischemic stroke. Hum Brain Mapp. 42, 2278–2291.
Bonkhoff, A.K., et al., 2021b. Dynamic connectivity predicts acute motor impairment and recovery post-stroke. Brain Commun. 3, fcab227.
Brett, M., Leff, A.P., Rorden, C., Ashburner, J., 2001. Spatial normalization of brain images with focal lesions using cost function masking. Neuroimage 14, 486–500.
Bullmore, E., Sporns, O., 2009. Complex brain networks: graph theoretical analysis of structural and functional systems. Nat. Rev. Neurosci. 10, 186–198.
Calamante, F., Smith, R.E., Liang, X., Zalesky, A., Connelly, A., 2017. Track-weighted dynamic functional connectivity (TW-dFC): a new method to study time-resolved functional connectivity. Brain Struct. Funct. 222, 3761–3774.
Carrera, E., Tononi, G., 2014. Diaschisis: past, present, future. Brain 137, 2408–2422.
Carter, A.R., et al., 2010. Resting interhemispheric functional magnetic resonance imaging connectivity predicts performance after stroke. Ann. Neurol. 67, 365–375.
Carter, A.R., Shulman, G.L., Corbetta, M., 2012. Why use a connectivity-based approach to study stroke and recovery of function? Neuroimage 62, 2271–2280.
Chen, J., et al., 2018. Alterations of static functional connectivity and dynamic functional connectivity in motor execution regions after stroke. Neurosci. Lett. 686, 112–121.
Cohen, J.R., 2018. The behavioral and cognitive relevance of time-varying, dynamic changes in functional connectivity. Neuroimage 180, 515–525.
Corbetta, M., et al., 2015. Common behavioral clusters and subcortical anatomy in stroke. Neuron 85, 927–941.
Coscia, M., et al., 2019. Neurotechnology-aided interventions for upper limb motor rehabilitation in severe chronic stroke. Brain 142, 2182–2197.
Delavari, F., et al., 2021. Dysmaturation observed as altered hippocampal functional connectivity at rest is associated with the emergence of positive psychotic symptoms in patients with 22q11 deletion syndrome. Biol. Psychiatry.
Drysdale, A.T., et al., 2017. Resting-state connectivity biomarkers define neurophysiological subtypes of depression. Nat. Med. 23, 28–38.
Duncan, E.S., Small, S.L., 2018. Changes in dynamic resting state network connectivity following aphasia therapy. Brain Imag. Behav. 12, 1141–1149.
Fisher, R.A., 1936. The use of multiple measurements in taxonomic problems. Ann. Eugen. 7, 179–188.
Fox, M.D., et al., 2005. The human brain is intrinsically organized into dynamic, anticorrelated functional networks. Proc. Natl. Acad. Sci. U.S.A. 102, 9673–9678.
Fred, A.L., Jain, A.K., 2002. Data Clustering Using Evidence Accumulation in. IEEE, pp. 276–280.
Fred, A.L., Jain, A.K., 2005. Combining multiple clusterings using evidence accumulation. IEEE Trans. Pattern Anal. Mach. Intell. 27, 835–850.
Griffis, J.C., Metcalf, N.V., Corbetta, M., Shulman, G.L., 2019. Structural disconnections explain brain network dysfunction after stroke. Cell Rep. 28, 2527–2540.
Griffis, J.C., Metcalf, N.V., Corbetta, M., Shulman, G.L., 2020. Damage to the shortest structural paths between brain regions is associated with disruptions of resting-state functional connectivity after stroke. Neuroimage 210, 116589.
Guggisberg, A.G., Koch, P.J., Hummel, F.C., Buetefisch, C.M., 2019. Brain networks and their relevance for stroke rehabilitation. Clin. Neurophysiol. 130, 1098–1124.
Haller, S., Lovblad, K.-.O., Giannakopoulos, P., Van De Ville, D., 2014. Multivariate pattern recognition for diagnosis and prognosis in clinical neuroimaging: state of the art, current challenges and future trends. Brain Topogr. 27, 329–337.
Hu, J., et al., 2018. Dynamic network analysis reveals altered temporal variability in brain regions after stroke: a longitudinal resting-state fMRI study. Neural. Plast. 2018.
Hutchison, R.M., et al., 2013. Dynamic functional connectivity: promise, issues, and interpretations. Neuroimage 80, 360–378.
Karahanoğlu, F.I., Van De Ville, D., 2015. Transient brain activity disentangles fMRI resting-state dynamics in terms of spatially and temporally overlapping networks. Nat. Commun. 6, 1–10.
Karahanoğlu, F.I., Van De Ville, D., 2017. Dynamics of large-scale fMRI networks: deconstruct brain activity to build better models of brain function. Curr. Opin. Biomed. Eng. 3, 28–36.
Karahanoğlu, F.I., Caballero-Gaudes, C., Lazeyras, F., Van De Ville, D., 2013. Total activation: fMRI deconvolution through spatio-temporal regularization. Neuroimage 73, 121–134.
Kebets, V., et al., 2019. Somatosensory-motor dysconnectivity spans multiple transdiagnostic dimensions of psychopathology. Biol. Psychiatry 86, 779–791.
Khambhati, A.N., et al., 2019. Functional control of electrophysiological network architecture using direct neurostimulation in humans. Netw. Neurosci. 3, 848–877.
Kinany, N., Pirondini, E., Micera, S., Van De Ville, D., 2020. Dynamic functional connectivity of resting-state spinal cord fMRI reveals fine-grained intrinsic architecture. Neuron 108, 424–435.
Kinany, N., et al., 2022. Towards reliable spinal cord fMRI: assessment of common imaging protocols. Neuroimage, 118964.
Koch, P.J., Hummel, F.C., 2017. Toward precision medicine: tailoring interventional strategies based on noninvasive brain stimulation for motor recovery after stroke. Curr. Opin. Neurol. 30, 388–397.
Krakauer, J.W., 2004. Functional imaging of motor recovery after stroke: remaining challenges. Curr. Neurol. Neurosci. Rep. 4, 42–46.
Krakauer, J.W., 2007. Avoiding performance and task confounds: multimodal investigation of brain reorganization after stroke rehabilitation. Exp. Neurol. 204, 491–495.
Krishnan, A., Williams, L.J., McIntosh, A.R., Abdi, H., 2011. Partial Least Squares (PLS) methods for neuroimaging: a tutorial and review. Neuroimage 56, 455–475.
Lee, M.H., Smyser, C.D., Shimony, J.S., 2013. Resting-state fMRI: a review of methods and clinical applications. Am. J. Neuroradiol. 34, 1866–1872.
Muldoon, S.F., et al., 2016. Stimulation-based control of dynamic brain networks. PLoS Comput. Biol. 12, e1005076.
Nozais, V., Forkel, S.J., Foulon, C.J., Petit, L., de Schotten, M.T., 2021. Functionnectome: a framework to analyse the contribution of brain circuits to fMRI. bioRxiv.
Obando, C., Rosso, C., Siegel, J., Corbetta, M., Fallani, F.D.V., 2019. Temporal connection signatures of human brain networks after stroke. arXiv preprint arXiv:1907.10009.
Piguet, C., Karahanoğlu, F.I., Saccaro, L.F., Van De Ville, D., Vuilleumier, P., 2021. Mood disorders disrupt the functional dynamics, not spatial organization of brain resting state networks. NeuroImage: Clinical 32, 102833.
Pirondini, E., et al., 2020. Resting-state EEG topographies: reliable and sensitive signatures of unilateral spatial neglect. NeuroImage: Clinical, 102237.
Power, J.D., Barnes, K.A., Snyder, A.Z., Schlaggar, B.L., Petersen, S.E., 2012. Spurious but systematic correlations in functional connectivity MRI networks arise from subject motion. Neuroimage 59, 2142–2154.
Preti, M.G., Bolton, T.A., Van De Ville, D., 2017. The dynamic functional connectome: state-of-the-art and perspectives. Neuroimage 160, 41–54.
Ramsey, L., et al., 2017. Behavioural clusters and predictors of performance during recovery from stroke. Nature Hum. Behav. 1, 1–10.
Robb, R.A., Hanson, D.P., 1991. A software system for interactive and quantitative visualization of multidimensional biomedical images. Australas. Phys. Eng. Sci. Med. 14, 9–30.
Salvalaggio, A., De Filippo De Grazia, M., Zorzi, M., Thiebaut de Schotten, M., Corbetta, M., 2020. Post-stroke deficit prediction from lesion and indirect structural and functional disconnection. Brain 143, 2173–2188.
Siegel, J.S., et al., 2016. Disruptions of network connectivity predict impairment in multiple behavioral domains after stroke. Proc. Natl. Acad. Sci. 113, E4367–E4376.
Siegel, J.S., et al., 2018. *Re*-emergence of modular brain networks in stroke recovery. Cortex 101, 44–59.
Tarun, A., et al., 2020a. NREM sleep stages specifically alter dynamical integration of large-scale brain networks. iScience, 101923.
Tarun, A., Behjat, H., Bolton, T., Abramian, D., Van De Ville, D., 2020b. Structural mediation of human brain activity revealed by white-matter interpolation of fMRI. Neuroimage 213, 116718.
Tzourio-Mazoyer, N., et al., 2002. Automated anatomical labeling of activations in SPM using a macroscopic anatomical parcellation of the MNI MRI single-subject brain. Neuroimage 15, 273–289.
Van Den Heuvel, M.P., Pol, H.E.H., 2010. Exploring the brain network: a review on resting-state fMRI functional connectivity. Eur. Neuropsychopharmacol. 20, 519–534.
Ward, N.S., 2015. Does neuroimaging help to deliver better recovery of movement after stroke? Curr. Opin. Neurol. 28, 323–329.
Woo, C.-.W., Chang, L.J., Lindquist, M.A., Wager, T.D., 2017. Building better biomarkers: brain models in translational neuroimaging. Nat. Neurosci. 20, 365.
Yeh, F.C., et al., 2018. Population-averaged atlas of the macroscale human structural connectome and its network topology. Neuroimage 178, 57–68.
Yin, M., et al., 2020. Effects of rTMS treatment on cognitive impairment and resting-state brain activity in stroke patients: a randomized clinical trial. Front. Neural Circuits 14, 62.
Zöller, D., et al., 2017. Disentangling resting-state BOLD variability and PCC functional connectivity in 22q11. 2 deletion syndrome. Neuroimage 149, 85–97.
Zöller, D.M., et al., 2018a. Robust recovery of temporal overlap between network activity using transient-informed spatio-temporal regression. IEEE Trans. Med. Imag. 38, 291–302.
Zöller, D., et al., 2018b. Psychotic symptoms influence the development of anterior cingulate BOLD variability in 22q11. 2 deletion syndrome. Schizophr. Res. 193, 319–328.
Zöller, D., et al., 2019. Large-scale brain network dynamics provide a measure of psychosis and anxiety in 22q11. 2 deletion syndrome. Biol. Psychiatry 4, 881–892.
Zhang, C., Baum, S.A., Adduru, V.R., Biswal, B.B., Michael, A.M., 2018. Test-retest reliability of dynamic functional connectivity in resting state fMRI. Neuroimage 183, 907–918.
Zoeller, D., et al., 2019. Structural control energy of resting-state functional brain states reveals inefficient brain dynamics in psychosis vulnerability. bioRxiv, 703561.